Statistical Parameterization of Heterogeneous Oceanic Convection

CLAUDIA PASQUERO

Division of Geological and Planetary Sciences, California Institute of Technology, Pasadena, California

ELI TZIPERMAN

Earth and Planetary Sciences and Division of Engineering and Applied Sciences, Harvard University, Cambridge, Massachusetts

(Manuscript received 17 October 2005, in final form 24 January 2006)

ABSTRACT

A statistical convective adjustment scheme is proposed that attempts to account for the effects of mesoscale and submesoscale variability of temperature and salinity typically observed in the oceanic convective regions. Temperature and salinity in each model grid box are defined in terms of their mean, variance, and mutual correlations. Subgrid-scale instabilities lead to partial mixing between different layers in the water column. This allows for a smooth transition between the only two states (convection on and convection off) allowed in standard convective adjustment schemes. The advantage of the statistical parameterization is that possible instabilities associated with the sharp transition between the two states, which are known to occasionally affect the large-scale model solution, are eliminated. The procedure also predicts the generation of correlations between temperature and salinity and the presence of convectively induced upgradient fluxes that have been obtained in numerical simulations of heterogeneous convection and that cannot be represented by standard convective adjustment schemes.

1. Introduction

Ocean general circulation model (GCM) equations are written for the gridbox-averaged quantities, and the subgrid-scale variability of temperature, salinity, and velocities is often parameterized in the form of eddy viscosity and diffusivity. Observations in regions of deep oceanic convection, such as the Labrador Sea, show that temperature T and salinity S fields have small- and mesoscale variability (Lilly et al. 2003), which is believed to play an important role in the convective process. Mesoscale cyclonic eddies are considered key ingredients in the preconditioning process, acting to reduce the vertical stability in the water column and set the location of the convective plumes (DiBattista et al. 2002). Convective mixing is associated with vertical plumes within the preconditioned region, and with nearly isopycnal slantwise motion associated with the baroclinic instability of the convectively induced geostrophic rim current around the convecting chimney (Jones and Marshall 1993; Legg and Marshall 1993). The final state of a convective event is characterized by a rich horizontal structure of mixed and stratified water, with patches on scales of tens of kilometers and less [observed in polar convective regions, see Schott et al. (1994) and Lilly et al. (1999); studied in numerical models, see Jones and Marshall (1993), Legg and Marshall (1993), and DiBattista and Majda (2000)].

Convection is therefore both affected by small-scale processes and also creates small-scale anomalies, whose scales are significantly smaller than a grid cell in a typical GCM. Given that temperature and salinity vary horizontally within the area of a given model grid cell, it is possible for the stratification to become unstable at some locations within the area of a model grid cell, even if the gridcell average is stably stratified. Yet, ocean convection parameterizations (which are required, as the resolution of models is usually too coarse to resolve convection) do not normally take this into account explicitly. The effect of vertical plumes results mainly in the homogenization of the water column, probably without a vertical transport of mass (Send and Marshall 1995). Current convection parameterizations in GCMs are based on the gridcell mean static stability of the

Corresponding author address: Claudia Pasquero, Department of Earth System Science, University of California, 3224 Croul Hall, Irvine, CA 92697-3100.
E-mail: claudia.pasquero@uci.edu

DOI: 10.1175/JPO3008.1

vertical column, and remove static instability either instantaneously (Bryan 1969; Marotzke 1991; Rahmstorf 1993) or on a finite adjustment time scale (Klinger et al. 1996). The differences between mixing adjustment schemes and enhanced vertical diffusivity schemes are not significant (Klinger et al. 1996; Marshall and Schott 1999), indicating that the instantaneous removal of instabilities is a reasonable assumption.

Alternatively, a number of vertical mixing parameterizations based on turbulence closure theories have been introduced, with the aim of representing the dynamics of the surface boundary layer in presence of both stable and unstable stratifications. Two commonly used turbulent closures in ocean models are the Mellor–Yamada 2.5-level scheme (MY2.5; Mellor and Yamada 1982), which includes a prognostic equation for the kinetic energy of the unresolved scales, and the K-profile parameterization (KPP; Large et al. 1994), which includes a nonlocal term in the expression for the turbulent diffusivity in the presence of unstable stratification (convective regime) and is meant to represent the effects of plumes or eddies that traverse large vertical distances. KPP seems to be the only parameterization used in ocean models that allows for upgradient fluxes. A recently introduced turbulence closure model (Canuto et al. 2001, 2002) was tested under deep convection conditions (Canuto et al. 2004).

In this paper, we suggest a statistical convection parameterization that accounts for possible unresolved static instabilities on a subgrid scale. Specifically, if the gridbox-average density at a given location is $\overline{\rho}$, then the actual density variations within the area represented by the grid box is described by a probability density function (PDF). This allows us to calculate the probability that there are subgrid locations that are statically unstable even if the density profile in the model, based on $\overline{\rho}$, is stable. This probability, in turn, is used to derive the effects of the subgrid-scale convection on the resolved grid-averaged temperature, salinity, and density. This approach is similar in its philosophy (although not in its general outline nor implementation) to that used for deriving fractional cloud cover from an appropriate PDF in state-of-the-art statistical cloud parameterizations (e.g., Bony and Emanuel 2001; Jakob and Miller 2004; Randall 1989; Tompkins 2002).

Standard convection schemes mix the water vertically only when the vertical stratification based on the gridcell averages becomes unstable. This is therefore a discontinuous parameterization as a function of the gridcell-averaged temperature and salinity. The statistical parameterization is motivated by two different needs, both arising from the discontinuous nature of the standard convection parameterizations. As explained below, the statistical convection parameterization is smooth in the gridcell-averaged temperature and salinity. It may therefore prevent the spatially and temporally intermittent behavior of convection in OGCMs that is normally seen in GCM runs and seems to result from the discontinuous nature of standard convection schemes. The on–off switch of the convective adjustment process is known to create unphysical grid-scale instabilities (Cessi 1996), and to lead to temporal and grid-scale spatial variability (e.g., Hirschi et al. 1999; Lenderink and Haarsma 1994; Marotzke 1991; Rahmstorf 1995) that are strongly sensitive to numerical errors, initial conditions, and spatial and temporal resolution (Cessi and Young 1996; Titz et al. 2004). The second motivation arises from the difficulties caused by the standard switch convection parameterizations to the use of an adjoint of the ocean GCM (e.g., Tziperman and Thacker 1989). Because switch convection parameterizations are not differentiable, the adjoint may be ill-defined in convection areas and this may prevent its use for both sensitivity and data assimilation purposes. The nondifferentiability of the convection applies to both convection schemes that are based on the use of instantaneous mixing of unstable stratification and those based on the use of implicit vertical diffusion solution of the equations, with the vertical mixing coefficients made large when the density profile is unstable.

The development of the statistical convection scheme is only one of the two main objectives of this paper. The second objective is to investigate the role of convection in creating correlations between temperature and salinity anomalies. Density-compensated temperature and salinity anomalies have been observed in the mixed layer (e.g., Rudnick and Ferrari 1999), and their existence has been attributed to the selective elimination of uncompensated anomalies by processes that depend on the buoyancy gradients (Chen and Young 1995; Ferrari and Young 1997). Recently, Legg and McWilliams (2000) observed the selective generation of compensated temperature and salinity anomalies in a numerical study of convection in the presence of a temperature and salinity stratification.

Here, we examine how the generation of correlated T and S anomalies is obtained by mixing in heterogeneous conditions, and we find a significant appearance of compensated anomalies. In some specific conditions, negative correlations, corresponding to temperature and salinity anomalies that enhance each other to create maximal density anomalies, are obtained. We also investigate the mean effect of subgrid-scale convection on the vertical fluxes of heat and salt, obtaining upgradient salinity fluxes in polarlike convection. Upgradient fluxes have been observed in numerical simulations of heterogeneous convection (Legg and McWilliams 2000), but they cannot be parameterized in term of standard convective adjustments, as perfect homogenization (reduction of any gradient) is the end state of the standard convective mixing parameterizations. The parameterization proposed here can produce such upgradient fluxes.

In the following sections we introduce the statistical representation of subgrid-scale static instabilities (section 2) and show how to calculate the effects of this subgrid-scale convection on the resolved gridbox-averaged temperature and salinity. We then discuss the temporal evolution of the PDFs for the temperature and salinity anomalies within a grid box after a convection event (section 3). Next, we demonstrate the scheme using a column model (section 4), perform some sensitivity tests (section 5), and conclude in section 6.

2. Statistical convective instability

Consider two vertically adjacent ocean model levels, with thicknesses z_t for the top level and z_b for the bottom one. The density in each layer is assumed homogeneous in the vertical direction, but lateral anomalies may be present, and they are characterized in terms of the PDFs $P_t(\rho)$ and $P_b(\rho)$, whose mean values are the gridbox-averaged densities $\overline{\rho}_t$ and $\overline{\rho}_b$. The stratification is usually considered statically stable if $\overline{\rho}_t < \overline{\rho}_b$. However, some portions of the grid box may be statically unstable if the density anomalies in the two layers are such that the local density in the top layer is larger than the local density in the bottom layer. A parcel in the top layer with density ρ_t has a probability $P_{\text{unstable}}(\rho_t) = \int_{-\infty}^{\rho_t} d\rho_b\, P_b(\rho_b)$ of being denser than the water below, assuming that the anomalies in the two layers are uncorrelated (this assumption is further discussed below). Overall, the probability of having the density in the top layer larger than the density in the bottom layer is given by the sum of $P_{\text{unstable}}(\rho_t)$ over any density ρ_t in the top layer, weighted by the probability $P_t(\rho_t)$. This, by definition, is the probability of convection in the two-layer gridbox system:

$$
\begin{aligned}
P_{\text{conv}} &= P(\rho_t > \rho_b) \\
&= \int_{-\infty}^{\infty} d\rho_t\, P_t(\rho_t) \int_{-\infty}^{\rho_t} d\rho_b\, P_b(\rho_b) \\
&= \int_{-\infty}^{\infty} d\rho_t \int_{-\infty}^{\infty} d\rho_b\, H(\rho_t - \rho_b) P_t(\rho_t) P_b(\rho_b). \qquad (1)
\end{aligned}
$$

Here, the Heaviside function depends on the difference in density between the two levels: $H(\rho_t - \rho_b)$ is zero for $\rho_b > \rho_t$ and one otherwise, and therefore selects only the convectively unstable values of the top and bottom densities in Eq. (1). Note that the probability P_{conv} can be different from zero even when the mean density in the upper layer is smaller than the mean density in the lower layer. We refer to the cases in which the convection probability P_{conv} is different from zero as *statistically* unstable.

a. *Probability distribution functions of temperature and salinity*

Statistical stability depends on density stratification only, and not on potential temperature and salinity stratifications individually. However, ocean models use equations for salinity and potential temperature, and the convective parameterization scheme therefore needs to be given in terms of salinity and temperature distributions. In the following, we shall use a linearized equation of state to express density as a function of temperature and salinity:

$$\rho = \rho_0[1 - \alpha(\theta - \theta_0) + \beta(S - S_0)]. \qquad (2)$$

This choice allows us to find analytic expressions for the effects of the statistical convective scheme. The linearization may be done about the local gridbox-averaged temperature and salinity, so that the error introduced by not considering the full nonlinear equation of state is minimal.

The temperature and salinity distributions are described in terms of their mean values, $\overline{\theta}$ and $\overline{S}$, and their standard deviations, σ_θ and σ_S. Considering that subgrid-scale anomalies are created by many diverse and independent processes such as mesoscale oceanic variability and wind bursts, we assume that temperature and salinity distributions are described by Gaussian functions. We further allow for cross correlation between temperature and salinity:

$$\eta = \frac{\text{cov}(\theta, S)}{\sigma_\theta \sigma_S} = \frac{\overline{\theta S} - \overline{\theta}\,\overline{S}}{\sigma_\theta \sigma_S}. \qquad (3)$$

Positive correlations between temperature and salinity indicate that anomalously warm water is anomalously salty, and vice versa. The variance of density, $\Sigma^2 = \rho_0^2(\alpha^2\sigma_\theta^2 + \beta^2\sigma_S^2 - 2\alpha\beta\eta\sigma_\theta\sigma_S)$, is largest for given temperature and salinity distributions, when θ and S are perfectly anticorrelated ($\eta = -1$).

The distribution of temperature and salinity in each layer is therefore written as

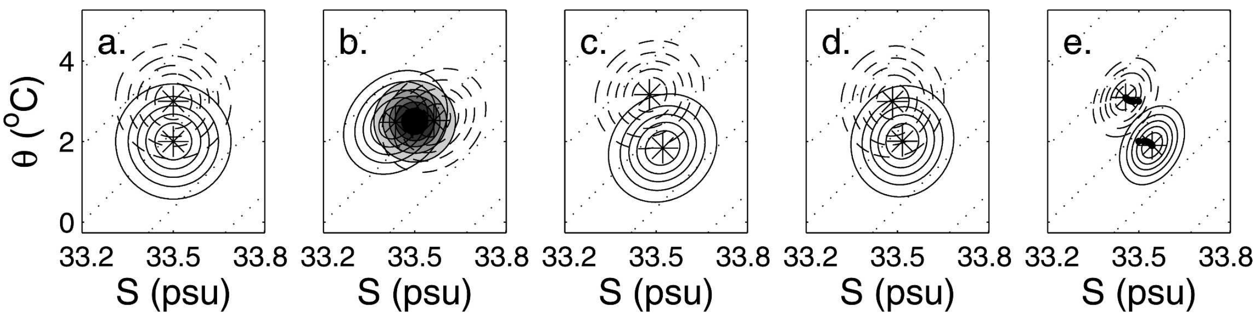

FIG. 1. An example of using the procedure described in section 2b. (a) Shown are contour plots of the two PDFs for two adjacent vertical levels before a convection event, as a function of the potential temperature and salinity in each level. Density contours are shown by the dotted lines. The mean stratification is stable, as seen by the fact that the top PDF (dashed lines) is centered about a lighter density than the bottom PDF (solid lines; mean values indicated by asterisks). However, convection occurs between the two levels on a subgrid scale. The probability of convection here is $P_{\mathrm{conv}} = 0.254$. (b) The PDFs for the convecting portion of the top (dashed) and bottom (solid) layers. Mean values and second-order moments have been obtained from Eqs. (6) and (7). The PDF for the mixed convecting region, as a result of the mixing of the top and bottom portions, is shown by the shaded area [first- and second-order moments of this distributions given by Eqs. (8) and (9)]. (c) The PDFs for the nonconvecting regions, defined by the mean values and variances in Eqs. (10) and (11). (d) The PDFs for each layer after the first iteration of the convective scheme, defined by the first- and second-order moments of Eqs. (12) and (13). Note that the vertical stratification has been stabilized, by increasing (decreasing) the salinity of the bottom (top) layer; convection in this case has slightly warmed (cooled) the bottom (top) layer. The probability for convection has not been completely removed, but it has reduced to $P_{\mathrm{conv}} = 0.18$, corresponding to about a 25% reduction in the static instability. (e) The PDFs after the completion of the entire convective scheme (repetition of steps 1–4 in section 2b until the probability of convection has been reduced below the threshold $P_{\mathrm{conv}} = 0.01$). The average stability of the two-layer system has increased, and the distributions of θ and S have been modified (smaller variances and positive correlations) so that the probability of convection became very small. Here, the initial conditions are $\overline{\theta}_t = 3°\mathrm{C}$, $\overline{\theta}_b = 2°\mathrm{C}$, $\overline{S}_t = \overline{S}_b = 33.5$ psu, $\sigma_{\theta,t} = \sigma_{\theta,b} = 0.75°\mathrm{C}$, $\sigma_{S,t} = \sigma_{S,b} = 0.1$ psu (so that $\alpha\sigma_\theta = \beta\sigma_S$), and $\eta_t = \eta_b = 0$. The final conditions are $\overline{\theta}_t = 3.1°\mathrm{C}$, $\overline{\theta}_b = 1.9°\mathrm{C}$, $\overline{S}_t = 33.45$, $\overline{S}_b = 33.55$ psu, $\sigma_{\theta,t} = \sigma_{\theta,b} = 0.5°\mathrm{C}$, $\sigma_{S,t} = \sigma_{S,b} = 0.05$ psu, and $\eta_t = \eta_b = 0.31$.

$$P(\theta, S; \sigma_\theta, \sigma_S, \eta, \overline{\theta}, \overline{S}) = P(\theta, S) = \frac{1}{2\pi\sigma_\theta\sigma_S\sqrt{1-\eta^2}}\exp\left\{-\frac{1}{1-\eta^2}\left[\frac{(\theta-\overline{\theta})^2}{2\sigma_\theta^2} + \frac{(S-\overline{S})^2}{2\sigma_S^2} - \eta\frac{(\theta-\overline{\theta})(S-\overline{S})}{\sigma_\theta\sigma_S}\right]\right\}, \tag{4}$$

and subscripts t and b will be used to characterize the top and bottom distributions. Two example of distributions are shown in Fig. 1a.

The probability of convection [Eq. (1)] can now be expressed in terms of double integrals over potential temperature and salinity for each layer, and the equation of state, Eq. (2), is used to calculate the argument of the Heaviside function:

$$P_{\mathrm{conv}} = \int_{-\infty}^{+\infty}\int_{-\infty}^{\infty} d\theta_t\, dS_t\, P_t(\theta_t, S_t) \times \int_{-\infty}^{+\infty}\int_{-\infty}^{\infty} d\theta_b\, dS_b\, P_b(\theta_b, S_b) H(\rho_t - \rho_b). \tag{5}$$

b. Convective mixing

Given the above probability of convective mixing, we can calculate the mean temperature and salinity over the convecting regions within a grid cell as

$$\langle X_t\rangle = P_{\mathrm{conv}}^{-1}\int_{-\infty}^{\infty}\int_{-\infty}^{\infty} dS_t\, d\theta_t \times \int_{-\infty}^{\infty}\int_{-\infty}^{\infty} dS_b\, d\theta_b\, H(\rho_t - \rho_b) X_t P_t(\theta_t, S_t) P_b(\theta_b, S_b), \tag{6}$$

where X is either θ or S and angular brackets indicate an average over the convecting fraction of the layer surface area (see notation in Table 1). The corresponding second-order moments are

$$\langle X_t Y_t\rangle = P_{\mathrm{conv}}^{-1}\int_{-\infty}^{\infty}\int_{-\infty}^{\infty} dS_t\, d\theta_t \times \int_{-\infty}^{\infty}\int_{-\infty}^{\infty} dS_b\, d\theta_b\, H(\rho_t - \rho_b) X_t Y_t P_t(\theta_t, S_t) \times P_b(\theta_b, S_b), \tag{7}$$

TABLE 1. Notation for different averages used within a grid cell.

Notation	Meaning	Equation
$\overline{()}$	Gridcell average	
$\tilde{()}$	Average over nonconvecting area within grid cell	10
$\langle()\rangle$	Average over convection area within grid cell	6
$()'$	Value after one iteration of convective mixing	12

where X and Y are either θ or S, allowing us to calculate $\langle\theta_t^2\rangle$, $\langle S_t^2\rangle$, and $\langle\theta_t S_t\rangle$ over the convecting region. The mean and second-order moments of convecting water from the bottom layer are calculated similarly.

We next assume that convecting water from the two layers becomes vertically homogenized (only within the convecting areas of a grid cell). Salt content and potential temperature are assumed to be conserved by the convective mixing [ignoring the small effect due to the fact that turbulent mixing actually conserves enthalpy rather than potential temperature; see Fofonoff (1962); McDougall (2003)]. Mixing between top water with temperature θ_t and salinity S_t and bottom water with temperature θ_b and salinity S_b creates homogenized water with temperature $(z_t\theta_t + z_b\theta_b)/(z_t + z_b)$ and salinity $(z_tS_t + z_bS_b)/(z_t + z_b)$. The averaged properties over the convective portion of the gridbox surface area after the mixing between the convecting fractions of top- and bottom-layer distributions are therefore

$$\langle X\rangle = P_{\text{conv}}^{-1}\int_{-\infty}^{\infty}\int_{-\infty}^{\infty} dS_t\, d\theta_t \int_{-\infty}^{\infty}\int_{-\infty}^{\infty} dS_b\, d\theta_b\, H(\rho_t - \rho_b)\frac{z_tX_t + z_bX_b}{z_t + z_b}P_t(\theta_t, S_t)P_b(\theta_b, S_b) \quad \text{and} \tag{8}$$

$$\langle XY\rangle = P_{\text{conv}}^{-1}\int_{-\infty}^{\infty}\int_{-\infty}^{\infty} dS_t\, d\theta_t \int_{-\infty}^{\infty}\int_{-\infty}^{\infty} dS_b\, d\theta_b\, H(\rho_t - \rho_b)\frac{z_tX_t + z_bX_b}{z_t + z_b}\frac{z_tY_t + z_bY_b}{z_t + z_b}P_t(\theta_t, S_t)P_b(\theta_b, S_b). \tag{9}$$

These first and second moments define the assumed Gaussian PDFs of the temperature and salinity, and Fig. 1b shows these PDFs for the water in the convecting portion of each grid cell as well as that of the mixed water mass.

Similarly, the statistical properties of the water in the nonconvecting areas of each layer (indicated by the tilde) are

$$\tilde{X}_{t(b)} = (1 - P_{\text{conv}})^{-1}\int_{-\infty}^{\infty}\int_{-\infty}^{\infty} dS_t\, d\theta_t \int_{-\infty}^{\infty}\int_{-\infty}^{\infty} dS_b\, d\theta_b\, H(\rho_b - \rho_t)X_{t(b)}P_t(\theta_t, S_t)P_b(\theta_b, S_b) \quad \text{and} \tag{10}$$

$$\widetilde{XY}_{t(b)} = (1 - P_{\text{conv}})^{-1}\int_{-\infty}^{\infty}\int_{-\infty}^{\infty} dS_t\, d\theta_t \int_{-\infty}^{\infty}\int_{-\infty}^{\infty} dS_b\, d\theta_b\, H(\rho_b - \rho_t)X_{t(b)}Y_{t(b)}P_t(\theta_t, S_t)P_b(\theta_b, S_b). \tag{11}$$

Note that the sign of the argument in the Heaviside function in Eqs. (10) and (11) has been reversed. The PDFs for water in the nonconvecting region of each layer, obtained under the hypothesis of Gaussianity from the knowledge of the corresponding first- and second-order statistics, are shown in Fig. 1c.

Last, the new first and second moments after the convection (denoted by primes) are calculated for both layers by averaging over the convecting and nonconvecting regions in each layer:

$$\overline{X}'_{t(b)} = P_{\text{conv}}\langle X\rangle + (1 - P_{\text{conv}})\tilde{X}_{t(b)} \quad \text{and} \tag{12}$$

$$\overline{XY}'_{t(b)} = P_{\text{conv}}\langle XY\rangle + (1 - P_{\text{conv}})\widetilde{XY}_{t(b)}. \tag{13}$$

Given this weighted mean of the first and second moments of the temperature and salinity after the convection, we can calculate the new PDF by assuming again that it is Gaussian. Figure 1d shows the PDFs after partial mixing of waters initially characterized by the PDFs of Fig. 1a.

At the end of the procedure described so far, the PDFs for the top and bottom layers may still overlap (Fig. 1d), indicating that the instability has not been completely removed. The procedure is then iterated until the probability of convection is reduced below a given threshold (here, the threshold $P_{\text{conv}} < 1\%$ is used). The results after these iterations are shown in Fig. 1e.

In summary, the statistical convection parameterization is composed of the following steps:

1) compute the probability of convection P_{conv} between two nearby levels [Eq. (5)];
2) compute the gridbox mean, variance, and correlation of the temperature and salinity over the convecting and nonconvecting fractions in each layer before the convection [Eqs. (6), (7), (10), and (11)];
3) vertically homogenize temperature and salinity over the convective regions [Eqs. (8) and (9)];
4) compute the modified mean, variance, and correlation for the temperature and salinity after the convection and over the entire gridbox area for each layer [Eqs. (12) and (13)]; and
5) repeat steps 1–4 until P_{conv} becomes smaller than the specified threshold.

The appendix provides the analytic solution to the integrals for the mean and variance required for the above steps.

The effect of convection occurring in a portion of the grid area is in general to increase the mean density difference between the two layers, and to reduce the density variance in each layer. This occurs because convection selects the largest (smallest) density values in the top (bottom) layer, and replaces them with the mixed water that has smaller (larger) density. The net effect is to reduce density anomalies within each layer. In terms of temperature and salinity, a reduction of the density variance can happen in two main ways: by a reduction of the variances of θ and S individually, and by a modification of the correlations between θ and S. Even in the case of no correlation between θ and S before the convective event, the convection introduces some correlation, as it selects in each layer those values of the θ and S anomalies that sum to give a particularly large (or small) density. The positive correlations created in each layer in the convecting regions are then modified by the mixing process. Depending on the water characteristics of the nearby level, the whole process might result in the creation of either positive or negative correlations, as further discussed in section 4a below.

3. Evolution of temperature and salinity distributions

The variance and correlation of temperature and salinity within a given grid cell are clearly important quantities in the proposed scheme. Ocean GCMs do not normally predict the value of the second-order moments of the temperature and salinity distributions in each grid box. In the absence of a suitable closure theory that relates the values of σ and η to the first-order moments of the distributions and/or to other variables of the model, we attempt in this section to relate them to observations, and discuss their temporal evolution after the end of a convection event.

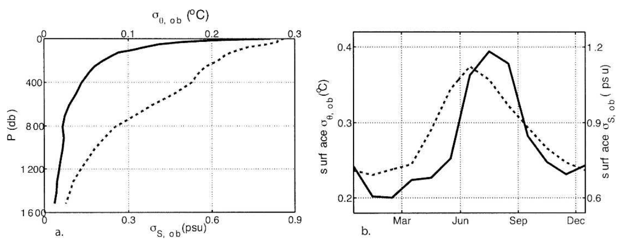

FIG. 2. High-latitude North Atlantic averaged vertical profiles of temperature and salinity standard deviations [from *WOA01* $1° \times 1°$ grid monthly dataset; Conkright et al. (2002)]. (a) Annual mean values of rms temperature (solid line) and salinity (dashed line). (b) Seasonal variation of the surface temperature (solid line) and salinity (dashed line) standard deviation.

Local temperature and salinity anomalies in the oceans are created by air–sea interactions, by ocean eddies, and by other ocean instabilities. Typically, variances are large at the surface and decrease with depth. Figure 2a shows typical potential temperature and salinity standard deviations ($\sigma_{\theta,\text{ob}}$ and $\sigma_{S,\text{ob}}$) found in the North Atlantic Ocean region, at latitudes north of 50°N and longitudes between 80°W and 20°E. This area includes the Labrador Sea and the Greenland Sea, where deep convection is known to occur in wintertime. The profiles of the annual mean values of $\sigma_{\theta,\text{ob}}$ and $\sigma_{S,ob}$ have been obtained by averaging the monthly root-mean-square (rms) values on $1° \times 1°$ boxes [*World Ocean Atlas 2001*, *WOA01*; Conkright et al. (2002)].

It is interesting to observe that the salinity anomalies in this area are responsible for most of the density anomalies, as $\beta\sigma_{S,\text{ob}}$ is more than 10 times the $\alpha\sigma_{\theta,\text{ob}}$ at the surface. The seasonal variations of the surface temperature and salinity standard deviations, for the same area, are shown in Fig. 2b. The surface anomalies increase in the summertime and are minimal in the winter months. The temperature variance increases in the summer months at the surface, but is constant below 100 m from the surface (not shown). The salinity variability is particularly large during the summer months (Fig. 2b), as sea ice melts and creates pockets of freshwater.

The observed rms values shown in Fig. 2 represent the *temporal* variability of the temperature and salinity within a $1° \times 1°$ square rather than the *spatial* variance required and used for the above parameterization. Given no other source of information about the spatial variances, we assume that the spatial variance within a $1° \times 1°$ square has the same vertical structure, but a smaller amplitude, which will be specified below. There are several reasons to assume that these observed variances are different from, and most likely larger than, the spatial variances σ_θ and σ_S required by the parameterization. A large part of the horizontal anomalies has coherent structure in the vertical direction. In other words, a region of particularly dense water at the surface is most likely located above a dense water column. We expect only a fraction of the total variance to actively affect the probability of convection. Since the convective parameterization presented here assumes that anomalies in different levels before the convection are not correlated, the values of the model restoring temperature and salinity standard deviations, σ_X^*, are significantly smaller than the observational values. The actual fraction ($\delta = \sigma_X^*/\sigma_{X,\mathrm{ob}}$) is considered a free parameter of the model and the sensitivity to δ will be examined in section 5. The value of δ is constrained by the requirement of obtaining a realistic frequency and intensity for the convective events. In the absence of appropriate data, the reference temperature–salinity correlation, η_{ob}, is assumed to be zero, but can clearly be considered different from zero when the procedure is used to parameterize a specific observed convective event.

After a convective event modifies the variance of the temperature and salinity anomalies, we assume that these anomalies are regenerated by the different processes mentioned above and gradually recover their initial values $\sigma_{X,\mathrm{ob}}$, η_{ob}. We assume that the processes responsible for the gradual recovery of the horizontal temperature and salinity anomalies are slower than the process of vertical convection and therefore happen over many model time steps. To represent this process, we use a gradual relaxation of the rms and correlation values to prespecified values (indicated by asterisks), which can depend on location, depth, and/or season:

$$\frac{d\sigma_X}{dt} = \gamma[\sigma_X^*(\mathbf{s}, t) - \sigma_X] \quad \text{and} \tag{14}$$

$$\frac{d\eta}{dt} = \gamma(\eta^* - \eta). \tag{15}$$

Here, $1/\gamma$ is the relaxation time scale and $\mathbf{s}$ is the position vector that defines the geographical location and depth of the grid box under consideration.

The recovery of the horizontal distribution of anomalies about the grid-averaged temperature and salinity occurs in all vertical levels and may therefore result in the regeneration of convective instabilities.

4. Testing the parameterization using a column model

To test the above parameterization in a framework that more closely resembles an ocean GCM, yet is simple enough to allow extensive testing, we now use a one-dimensional convection–diffusion model of a vertical water column that obeys the following equations:

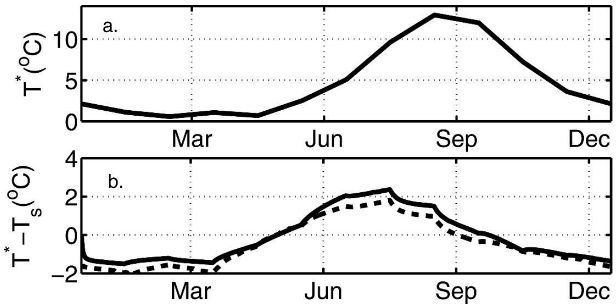

FIG. 3. (a) Restoring temperature for the surface box. (b) Air–sea heat flux for the statistical convection parameterization scheme, with $\delta = 0.05$ (solid line), and for the standard convective parameterization scheme (dashed line).

$$\frac{\partial\overline{\theta}}{\partial t} = \gamma(\overline{\theta^*} - \overline{\theta}) + k_v\frac{\partial^2\overline{\theta}}{\partial z^2}, \tag{16}$$

$$\frac{\partial\overline{S}}{\partial t} = \gamma(\overline{S^*} - \overline{S}) + k_v\frac{\partial^2\overline{S}}{\partial z^2}, \tag{17}$$

$$\frac{\partial\sigma_\theta}{\partial t} = \gamma(\sigma_\theta^* - \sigma_\theta), \tag{18}$$

$$\frac{\partial\sigma_S}{\partial t} = \gamma(\sigma_S^* - \sigma_S), \quad \text{and} \tag{19}$$

$$\frac{\partial\eta}{\partial t} = \gamma(\eta^* - \eta). \tag{20}$$

The variables $\overline{\theta}(z, t)$ and $\overline{S}(z, t)$ represent the gridbox mean potential temperature and salinity at a specified horizontal location. The first terms on the right-hand sides of Eqs. (16) and (17) are a relaxation to prescribed vertical profiles of temperature and salinity, meant to represent the effects of horizontal advection and diffusion. The prescribed profiles are chosen as the monthly mean potential temperature and salinity averaged over a $1° \times 1°$ box in the Labrador Sea at 51°W and 56°N. The monthly profiles are interpolated in time to the temporal resolution desired for the integration of Eqs. (16) and (17). The restoring rms values are $\sigma_X^* = \delta\sigma_{X,\mathrm{ob}}$, with $\sigma_{X,\mathrm{ob}}$ being the monthly rms typical of the North Atlantic region, interpolated in time, and $\delta = 0.05$ (see the discussion in the previous section). The relaxation correlation is chosen to vanish: $\eta^* = 0$. At the surface, temperature is relaxed to an "atmospheric" mean temperature (see Fig. 3a), which has the same mean value as the observed SST, but a seasonal variation 4 times as large. This creates a stronger surface temperature variability that triggers strong convection during the winter months and allows testing the parameterizations in both stable and unstable surface forcing conditions.

Convection is parameterized as described in section

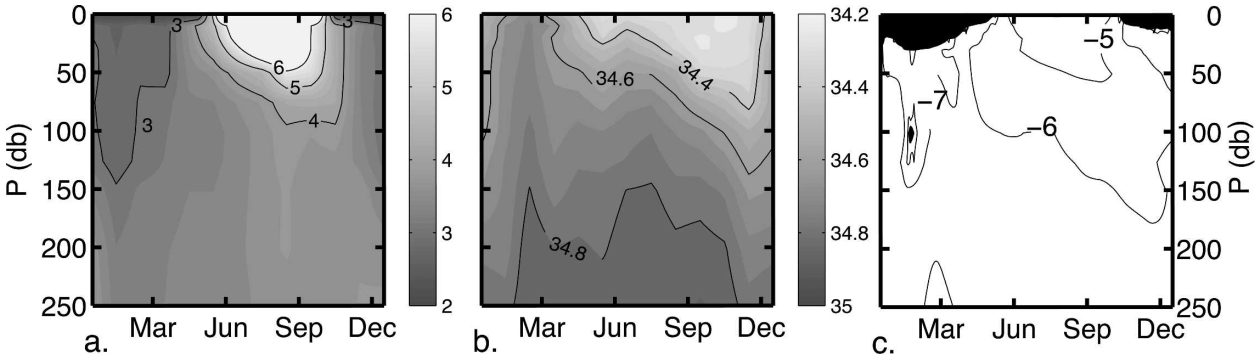

FIG. 4. Gridbox-average (a) temperature (°C), (b) salinity (psu), and (c) static stability (s^{-2}) in the upper 250 m, as function of depth and time, from the integration of Eqs. (16)–(20). In (c) black regions indicate static instability, and the numerical labels on contour lines indicate the exponent (e.g., −6 indicates 10^{-6} s^{-2}). Here, $\delta = 0.05$.

2: at every time step a check for statistical instability is performed between each two adjacent levels, and the convection scheme is applied if P_{conv} is larger than the threshold $P_{\text{conv}} = 0.01$.

The model is run for 1 yr, with $k_\upsilon = 1$ cm^2 s^{-1} and $\gamma = 0.1$ day^{-1}, with 25 vertical levels from the surface to 1500 m. Vertical resolution varies from 10 m at the surface to 100 m at the bottom of the column. The gridcell mean temperature, mean salinity, and mean static stability, $-1/\rho\partial\rho/\partial z$, in the upper 250 m are shown in Fig. 4. Thermal stratification is unstable in the winter months and stable in the summer months, while salinity stratification is almost always stable. This leads to strong convection during the winter months and very weak convection below the surface in the summer months, when the mean stratification is stable (Fig. 4c) but the anomalies can lead to weak (small P_{conv}) convective instability (Fig. 5c). In comparison with the convection patterns associated with a standard convection adjustment scheme shown in Fig. 5a (using the scheme of Rahmstorf 1993), the transitions between states of convection off and convection on (and vice versa) are much smoother. Note also that while the final state after the mixing associated with the standard convection adjustment is inevitably marginally stable from the statistical point of view, the gridbox-averaged stratification of the vertical column is statically stable after the statistical convection parameterization is used (Fig. 4c). The gridbox-averaged stratification is the only part of the convection parameterization seen by the model equations, and so these equations are not expected to suffer any artifacts due to residual instabilities after the convection event as parameterized by the statistical approach.

Heat and salt fluxes

During strong convection in wintertime, both gridcell mean salinity and potential temperature increase with depth (Fig. 6a), having opposite effects on the density stratification: salinity stratification is stable while temperature stratification is unstable. Salinity anomalies are very large, and they have a larger impact on the density variability than the temperature anomalies. Given that the salinity distribution in any given layer is scattered around the mean value, anomalously salty water can be found overlying anomalously freshwater, even if the mean S profile is stable. When this happens, the consequent convective vertical mixing is associated with a downward salt flux (Fig. 6b), which acts to stabilize the water column at any depth, and is up the mean salinity gradient. Note that the usual convective adjustment schemes cannot reproduce upgradient fluxes, as any gradient is removed by the mixing process that completely homogenizes the water. It will be interesting to look for observational evidence of upgradient fluxes in open-ocean convection; such fluxes have been obtained in numerical simulations of heterogeneous convection (Legg and McWilliams 2000).

Heat flux is directed upward in the top 300 m (Fig. 6b), as surface cold water is mixed with warmer water below by the mixing, while the heat flux is downward farther down the column, where the mean temperature stratification is slightly unstable. So the heat flux is always downgradient, leading to overall stabilization in the upper layer and destabilization at large depth. Overall, the density flux is always directed downward (not shown), as denser water from the upper layers is mixed with lighter water from the lower layers, increasing the stability of the vertical stratification. It is noteworthy that these results are consistent with the detailed simulations of three-dimensional heterogeneous convection by Legg and McWilliams (2000), who obtained downward salinity flux associated with baroclinic mixing for a monotonically increasing mean salinity with depth (Fig. 10 in Legg and McWilliams 2000). This behavior is thought to reflect the presence of a pre-

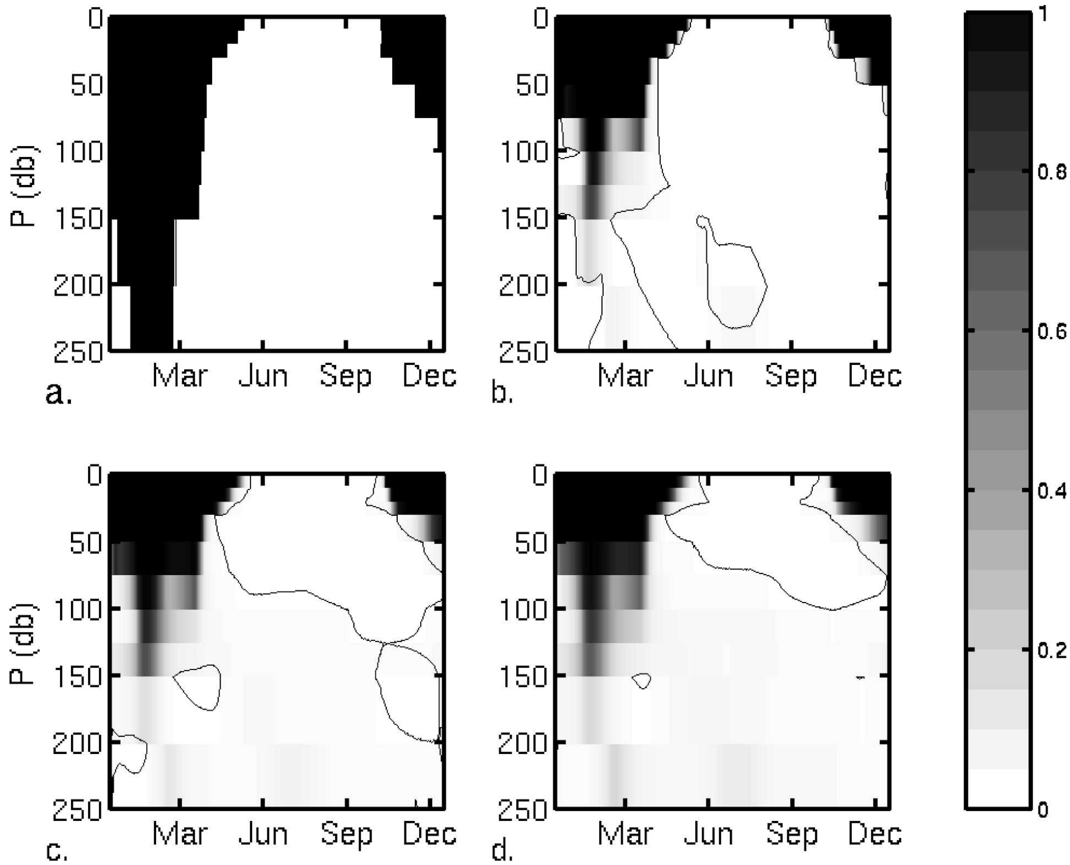

FIG. 5. Probability of convection in the upper 250 m, as a function of depth and time: (a) classic convection adjustment, implemented as in Rahmstorf (1993); (b) $\sigma^* = 0.01\sigma_{ob}$; (c) $\sigma^* = 0.03\sigma_{ob}$; and (d) $\sigma^* = 0.05\sigma_{ob}$. Lines indicate the boundaries between nonconvective and convective regions. Minimum P_{conv} for convecting is 0.01.

conditioned mesoscale eddy region, where salinity is larger than in the surrounding environment. Convective mixing in this case carries salt downward from the preconditioned area into the surrounding water.

In the context of the statistical representation of ocean convection, upgradient tracer flux can occur when the horizontal tracer variability is large relative to the difference of the mean tracer within the vertical mixing scale, h; that is, $|\partial\overline{X}/\partial z|h < \sigma_X$. Under such circumstances, water in the unstable region of a given level is replaced with mixed water whose characteristics are closer to the mean value of that level. In most cases, this results in a reduction of the tracer variability around the mean value of each layer. The opposite holds true if the mean vertical gradient is large, $|\partial\overline{X}/\partial z|h > \sigma_X$, where vertical mixing results in the generation of horizontal tracer variability. In this situation, the tracer flux is downgradient. For these reasons, convective mixing mostly increases the temperature variability (Fig. 7a) (apart from the upper layer in wintertime, when stratification is very weak and σ^*_θ is large), and reduces the salinity variances throughout the year (Fig. 7b). Density anomalies, as anticipated earlier, are always reduced by the convective mixing (Fig. 7c).

During convective mixing, new temperature salinity correlations are created. In general, in a layer with a given average temperature and salinity, mixing of a portion of it with warmer and saltier (or colder and fresher) water creates positive correlations, while mixing with warmer and fresher (or colder and saltier) water creates negative correlations. Large positive correlations are created during the strong convection of the winter months below the surface (Fig. 8), as the mean vertical gradients of temperature and salinity are both negative (θ and S increase with depth), while negative correlations can appear when thermal and salinity vertical gradients have opposite signs (as during the summer months below the mixed layer; see Fig. 8).

We show in Fig. 9 the formation of positive and negative correlations, due to vertical convective mixing between two adjacent vertical levels at 125-m depth, at two different times. During March (Figs. 9a and 9b) the average properties in the two-layer system are marginally stable, with warmer and saltier water below colder

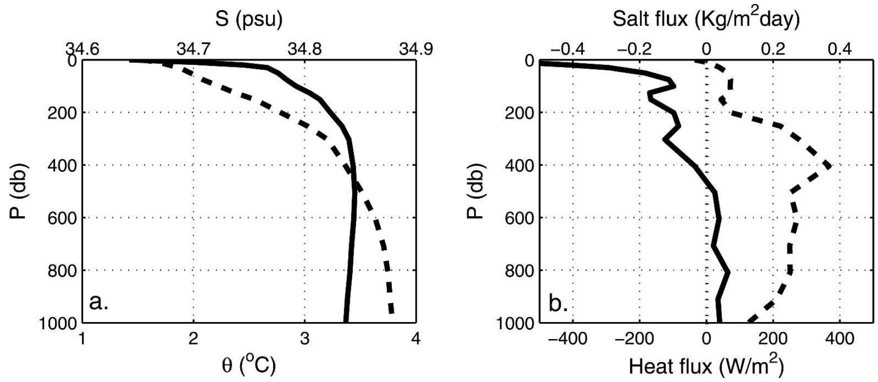

FIG. 6. February mean (a) potential temperature (solid line) and salinity (dashed line) vertical profiles, from the model output, and (b) heat (solid line) and salt (dashed line) convective fluxes. Positive values indicate downward fluxes. Heat flux is downgradient. Salt flux is upgradient. At any time step, fluxes of heat and salt are calculated from the convective mixing: the heat flux associated with the partial mixing between two nearby levels is computed as $\rho_0 c P_{\mathrm{conv}} z_t(\langle\theta\rangle - \langle\theta_t\rangle)/\Delta t$, where c is the specific heat of water and Δt is the time step. The flux is summed for all the iterations of the convective mixing computed at any time step. Similarly, the salt flux for each convective mixing iteration is $P_{\mathrm{conv}} z_t(\langle S\rangle - \langle S_t\rangle)/\Delta t$.

and fresher water, and $P_{\mathrm{conv}} = 48\%$. The upper layer is mixed with warmer and saltier water, introducing strong positive correlations. During September (Figs. 9c and 9d), the column is relatively well stratified, resulting in $P_{\mathrm{conv}} = 8.5\%$, for $\delta = 0.05$. The upper layer is then mixed with deeper water that is colder and saltier than the averaged properties at the upper level, resulting in the creation of negative correlations. Note that the density variability in each layer is reduced by the convective mixing despite the creation of negative correlations. We believe that the creation of negative correlations is an artifact of the convective mixing scheme, which for large enough variances predicts partial convective mixing in the summertime below the mixed layer. There is neither observational evidence nor theoretical support for such a convective mixing, suggesting that the variances of temperature and salinity that have been used are too large. We nevertheless show this case, with the aim of presenting the sensitivity of the parameterization to different parameter regimes.

5. Sensitivity study

In the previous section, the results of the application of the statistical convective parameterization to a column model have been described. The aim of this section is to analyze how these results differ from the results obtained using standard convective adjustment, based on the stability of the gridbox mean density (e.g.,

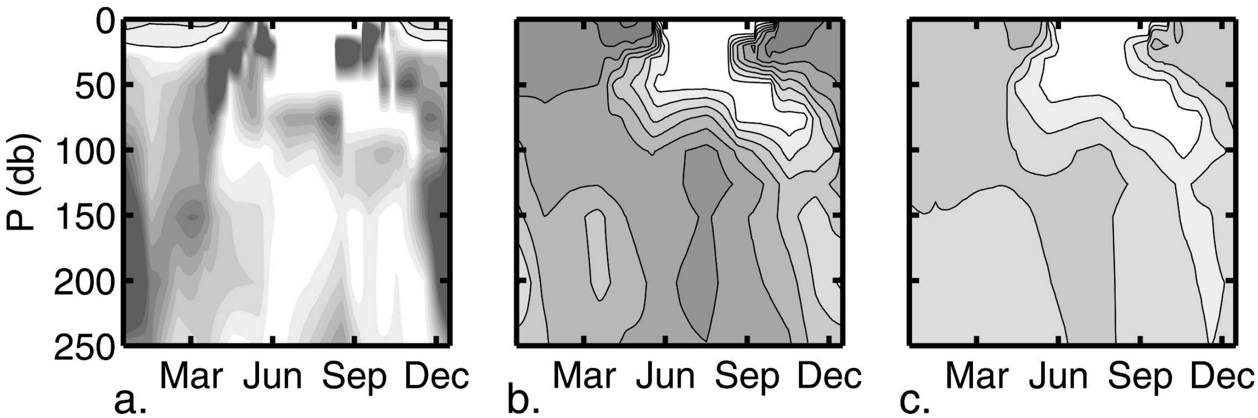

FIG. 7. Gridbox $(\sigma_X - \sigma_X^*)$ for (a) temperature (°C), (b) salinity (psu), and (c) density (kg m^{-3}) in the upper 250 m, as function of depth and time, from the integration of (16)–(20). Shading indicates the absolute value, $|\sigma_X - \sigma_X^*|$, with each tone of gray corresponding to a variation of 0.005 (in the respective units), starting from 0 (white). Negative regions, where the modeled variance is smaller than the restoring value, are marked with contour lines, while positive regions are only shaded. Convection mostly increases the temperature variances and reduces the salinity variances. Overall, the density anomalies are reduced by the convective mixing.

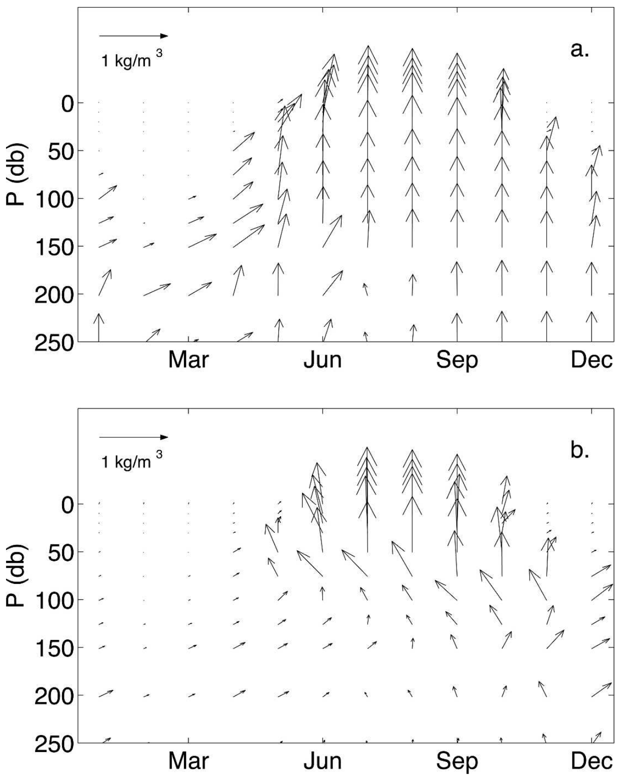

FIG. 8. Temperature–salinity correlation, η, created by the convective mixing. Length of arrow indicates density rms. Direction indicates the $\theta-S$ correlation: vertical means $\eta = 0$, horizontal refers to perfect correlation, either positive (arrow pointing right) or negative (arrow pointing left). (a) For $\delta = 0.01$, convection creates positive correlations; (b), for $\delta = 0.05$, the larger variability predicts weak convective mixing below the mixed layer in the summer months (see Fig. 5d), and negative correlations are here created.

Marotzke 1991; Rahmstorf 1993). Moreover, we also want to discuss the sensitivity of the results to the free parameter used in the statistical convective parameterization (δ; that is, the magnitude of the variances of θ and S), to the threshold value of $P_{\rm conv}$ below which no mixing is applied, and to the relaxation time γ^{-1}.

Consider first the effect of the convective scheme on the air–sea heat fluxes, when restoring temperature boundary conditions are used. The heat fluxes from the standard convective adjustment and the statistical convection parameterization are very similar (Figs. 3b and 3c). During summertime the surface layers are very stable, so that the air–sea heat fluxes are not affected by the convective parameterization chosen (no convection takes place). In the winter months, the heat loss to the atmosphere is larger (by about 25%) in the case of the standard convective adjustment scheme. This happens because the statistical convective scheme allows for a partial mixing ($P_{\rm conv} < 100\%$) even when the mean state is statically stable. The mixing between the warm subsurface water and the surface water is smaller than in the standard convective parameterization scheme, as some portions of the grid box are not statically unstable and are not affected by the convective mixing. This is an encouraging result, as one of the weak points of standard convective adjustment schemes is the sometimes excessive convection that upwells too much heat (Kim and Stossel 2001).

The probability of convection is shown in Fig. 5 for the upper 250 m, for different values of δ. For $\delta = 0$ the PDFs of temperature and salinity in each layer are delta functions, centered around the gridbox mean value. The probability of convection is either 0 or 1. As δ increases, the transition between states of convection on and states of convection off becomes smoother. Eventually, for large enough δ, partial mixing is found at any time and depth, resulting in an unrealistically strong mixing.

A quantitative measure of the degree of convection as a function of δ is reported in Fig. 10a. For $\delta = 0$ only profiles whose gridbox mean density profile is unstable convect. The number of convecting cells sharply increases for larger δ. The time and space average of the probability of convection increases with increased θ and S variability. The effect of increasing the specified θ and S variance on the value of $P_{\rm conv}$ in convecting cells depends on the stability of the mean profile: whenever the mean profile is stable, a larger value of δ allows for partial overlapping of the density distributions in the vertically adjacent cells, increasing the probability of convection. This effect can be seen in Fig. 10b, where below the first 100 m from the surface the annual mean convection probability increases with δ. On the other hand, when the mean profile is unstable, a larger variability of temperature and salinity reduces the probability of convection, as it becomes more likely to have anomalously light water on top of anomalously dense water (see upper layers in Fig. 10b). For this reason, as δ is increased, the mean probability of convection per convecting cells can be nonmonotonic. In particular, in Fig. 10 the mean value of $P_{\rm conv}$ over the convecting cells (i.e., 1 for $\delta = 0$) at first decreases, reaches a minimum, and then increases again as a large number of cell couples with a stable mean profile increase their unstable fraction.

As a first guess for the free parameter δ, we suggest a criterion based on the sensitivity of the mean value of $P_{\rm conv}$ per convecting cell: we use a value of δ in the range for which the average convection probability over convecting cells is relatively insensitive to the exact value of δ, that is, around its minimum. The specific value of δ, however, has to be refined by checking that

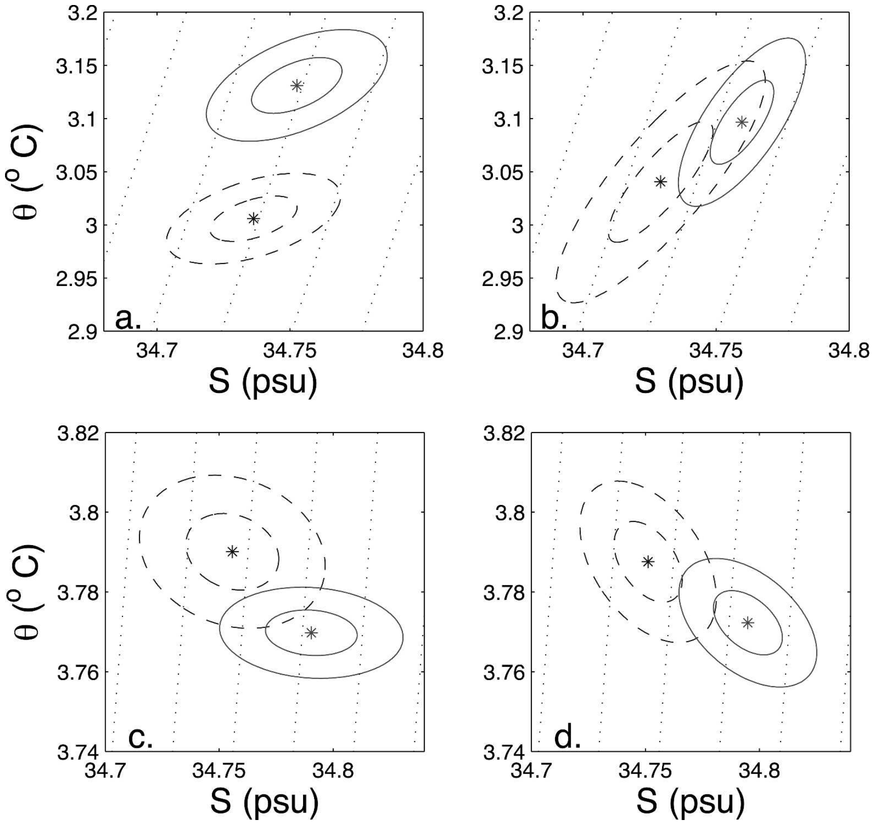

FIG. 9. Temperature and salinity properties in two nearby levels at 125 m below the surface (a), (c) before and (b), (d) after convection. Solid lines indicate the properties in the lower layer; dashed lines indicate the properties in the upper layer. Top row is for 15 Mar; bottom row is for 15 Sep. In the former case, convective mixing creates positive correlations; in the latter case convective mixing creates negative correlations. Here, $\delta = 0.05$.

the maximum convection depth and the occurrence of convective mixing are realistic. More work is needed to improve upon or better justify this choice. In particular, a way of explicitly accounting for vertical correlations in the temperature and salinity anomalies would greatly improve the statistical convection parameterization.

The dependence of the annual mean convecting fraction on the relaxation time γ^{-1} and to the specific threshold value chosen to apply convective mixing are shown in Figs. 10c and 10d. The procedure does not show a strong sensitivity to these parameters. In general, a larger threshold value for the initiation of convection is associated with a slightly smaller annual mean convecting fraction, as sometimes convection is not initiated. The dependence is however weak, as usually this results only in a small delay in the initiation of mixing.

The relaxation time, γ^{-1}, is important only for fast restoring, in which case the annual mean probability of convection is large, as the water column tends to be characterized by the restoring profiles, which are unstable during wintertime. For longer relaxation times, convective mixing becomes insensitive to the specific restoring time.

6. Discussion and conclusions

A parameterization of oceanic convection in general circulation models with a typical grid size of hundreds of kilometers needs to account for the small horizontal scale of the ocean convection, as well as for the lateral inhomogeneities associated with the vertical convection, such as those due to the baroclinic instabilities of the geostrophic rim current (see Marshall and Schott 1999). The statistical scheme described in this paper represents a crude attempt along these lines as an alternative to standard ocean convection schemes.

The proposed scheme calculates the probability of convection in a given grid cell and mixes only the unstable portion of the cell rather than the entire cell area. The scheme also calculates the effect of the convection on the variance of small-scale temperature and salinity

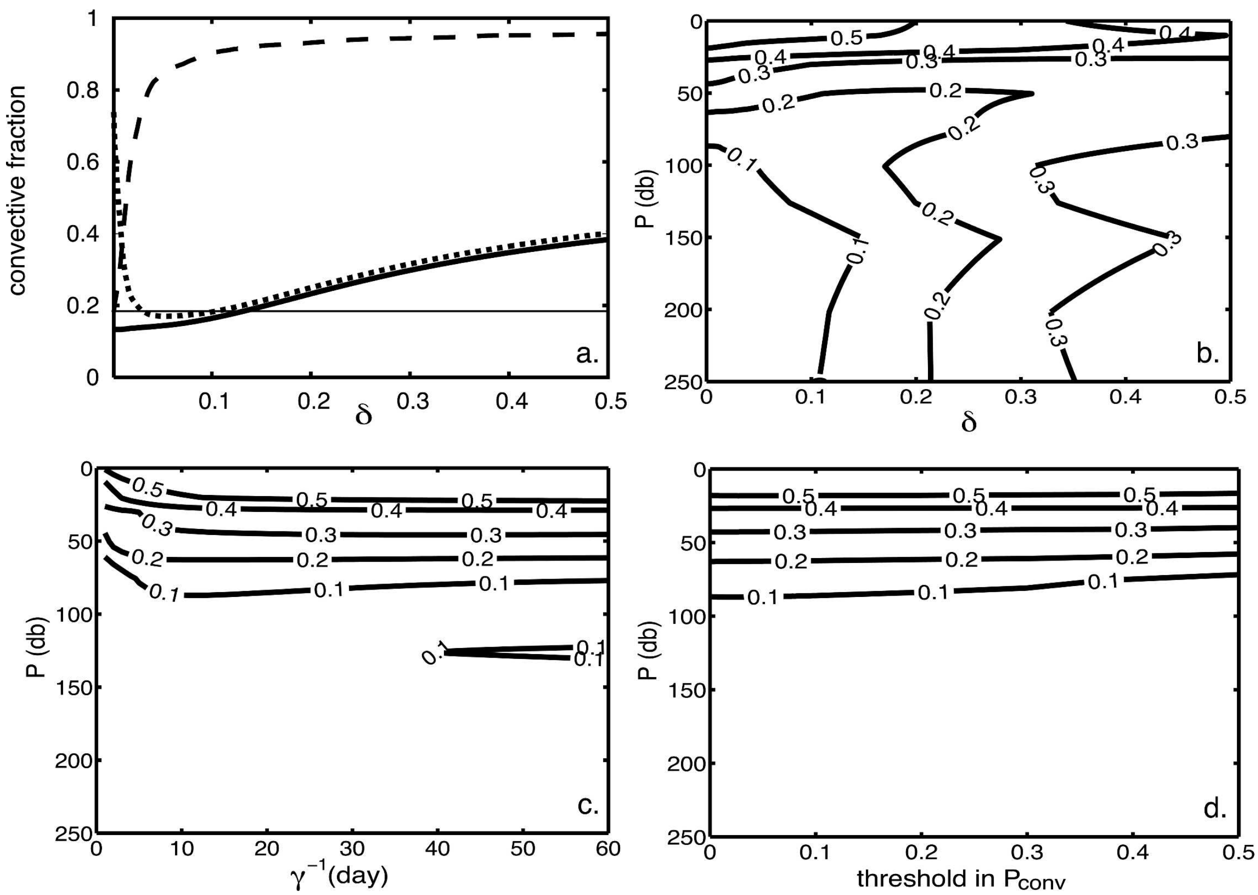

FIG. 10. (a) Fraction of the convective gridbox area as a function of δ. Thick solid line is the mean value of $P_{\rm conv}$ over the whole temporal duration of the integration and over any depth in the column. Dotted line is the mean value of $P_{\rm conv}$ over converting cells. Dashed line is the fraction of cells that are convecting. Horizontal line shows the fraction of convecting cells for the standard convective parameterization. As δ is decreased, the variance of the temperature and salinity distributions goes to zero. (b) Annual mean value of the fractional convecting area as a function of depth and δ. (c) Annual mean value of the fractional convective area as a function of depth and restoring time, γ^{-1}. (d) Annual mean value of the fractional convective area as a function of depth and threshold value in $P_{\rm conv}$, below which no mixing is applied.

distributions within a grid cell. The net effect of the statistical convective parameterization is, as expected, an increase of the static stability, via an increase in the difference between the mean densities in the top and bottom layers, as well as via a reduced anomaly variance in each layer, and the creation of θ–S correlations.

Convectively induced vertical fluxes of heat and salt and the creation of temperature and salinity correlations that are predicted by the statistical scheme seem consistent with numerical simulations of heterogeneous convection (Legg and McWilliams 2000). In particular, upgradient salt fluxes are reproduced by the statistical convective parameterization while they cannot be obtained by standard convective adjustment schemes, whose effect is always the homogenization of any property, eliminating any gradient. Positive correlations between temperature and salinity (density-compensated anomalies) arise directly from the mixing scheme.

Unfortunately, the parameterization proposed here still requires the specification of the second-order statistics of temperature and salinity. These must be specified somehow artificially based upon profiles of the rms variability. The parameterization is, in fact, very sensitive to the choice of these profiles, as is evident in the sensitivity to the parameter δ show in Fig. 10. Furthermore, we assume a relaxation to these specified profiles after a convection event, and this is not likely to be a physically realistic description of the development of these moments. Another limitation is that temperature and salinity are allowed to be correlated in the horizontal directions, but not in the vertical: we do not account for vertical coherence of the anomalies. For this reason, the actual values of the temperature and salinity variances that must be used in the parameterization are a small fraction, δ, of the observed values. The value of δ is a tunable parameter, and the sensitivity of the parameterization to its actual value has been investigated. For large values of δ, unrealistically large vertical mixing is introduced, and weak convection appears below the pycnocline in summer months. As this has no observational nor physical base, its appearance provides an upper value for the choice of the specified temperature and salinity variances. Further work and more physically sound criteria for the expressions of second-order moments may significantly improve the parameterization. One possibility is to estimate the spatial variability of the static stability from the observational data, so that vertical correlations would be taken into account. Another possible improvement is to couple of the stochastic parameterization to a turbulence closure model (Canuto et al. 2001, 2002). Last, one may envision combining the idea of a statistical convection parameterization with a physically based parameterization such as KPP (Large et al. 1994) by allowing some of the key parameters in KPP to be represented by a statistical PDF rather than by a single value.

The proposed parameterization may eliminate some of the problems found in standard convective adjustment schemes, which are based on the mean stratification of the water column. Cessi (1996) showed that convective adjustment schemes lead to instabilities of the smallest resolved horizontal scale, because mixing occurs in the vertical direction irrespective of the horizontal distributions of any given water property, with the effect of an amplification of the horizontal spatial gradients. Such instabilities may be eliminated by a statistical convective adjustment, as vertical mixing modifies gridbox mean properties more smoothly in time, and the lateral advection or diffusion has time to reduce the convectively formed spatial gradients. It may also be possible that the sensitivity to temporal and spatial model discretization (Cessi and Young 1996; Titz et al. 2004) may be eliminated. More research is needed to address these issues in detail and to examine how the stability of large-scale circulation may be affected by the statistical convective parameterization.

Acknowledgments. The trouble with Carl (according to author Tziperman): After my first year as a graduate student, during which Carl was my assigned adviser, I came into his office and announced that I would be happy to work with him but that I was not interested in data analysis or inverse methods. Carl looked amused and let me know that was just fine. A few months later, Carl carefully edited a terribly written draft manuscript I had given him, deleting every other word and rewriting the rest; he then deleted his name from the author list, telling me that an adviser does not necessarily need to be a coauthor on his students' papers. Some two years later, I was getting suspicious. With all these inverters around, and with Carl still never suggesting that I try working with inverse models, I became worried. Was I missing something? I ended up *wanting* to do an inverse model of something—anything. I proceeded, using Carl's generous help, suggestions, and ideas, and Carl still did not wish to be a coauthor. I have been working with inverse models ever since; this clearly would not have been the case had Carl ever suggested that I try this. It took me many years to appreciate just how unique Carl's ethics are. The trouble with Carl is that he is an impossible role model to follow. He is definitely an inspiration, though. Thank you, Carl.

Maria Rita d'Orsogna is gratefully acknowledged for having suggested the trick reported in Eq. (26). We thank two anonymous reviewers for their useful suggestions. Author Pasquero was supported by the Davidow's Discovery Fund, and author Tziperman was supported by the James McDonnell Foundation and by the NSF's Climate Dynamics Program (Grant ATM-0351123).

APPENDIX

Solution of the Integrals from Section 2

This appendix is devoted to the analytic solution of the integrals described in section 2. A FORTRAN subroutine that uses these integrals and applies the statistical convective parameterization to a column model was available online (http://www.ess.uci.edu/~cpasquer/research/stat_conv_param/stat_conv_param.F) at the time of writing.

The probability of convection [Eq. (1)] is

$$p_{\mathrm{conv}} = \int_{-\infty}^{\infty}\int_{-\infty}^{\infty} d\theta_t\, dS_t\, P_t(\theta_t, S_t)\int_{-\infty}^{\infty}\int_{-\infty}^{\infty} d\theta_b\, dS_b\, H(\rho_t - \rho_b)P_b(\theta_b, S_b) = \frac{1}{2}\left\{1 + \mathrm{erf}\left[\frac{\overline{\rho_t} - \overline{\rho_b}}{\sqrt{2(\Sigma_b^2 + \Sigma_t^2)}}\right]\right\}. \tag{A1}$$

The average temperature and salinity over the convecting regions are given by

$$\langle X_i \rangle = \overline{X}_i + P_{\text{conv}}^{-1} \frac{\sigma_{X,i}\rho_0(-\Psi_{X,i}^{\theta}\alpha\sigma_{\theta,i} + \Psi_{X,i}^{S}\beta\sigma_{S,i})}{\sqrt{2\pi(\Sigma_t^2 + \Sigma_b^2)}} e^{-\Delta\rho^2}, \tag{A2}$$

where X is either temperature θ or salinity S, the subscript i stands for either the top or bottom layers, and $\Psi_{X,i}^{\theta} = \eta_i$ when $X = S$ and is 1 otherwise; similarly, $\Psi_{X,i}^{S} = \eta_i$ when $X = \theta$ and is 1 otherwise; and $\Delta\rho^2 = (\overline{\rho}_t - \overline{\rho}_b)^2/2(\Sigma_t^2 + \Sigma_b^2)$.

Similarly, mean properties in the nonconvecting areas are

$$\tilde{X}_i = \overline{X}_i - \frac{1}{1 - P_{\text{conv}}} \frac{\sigma_{X,i}\rho_0(-\Psi_{X,i}^{\theta}\alpha\sigma_{\theta,i} + \Psi_{X,i}^{S}\beta\sigma_{S,i})}{\sqrt{2\pi(\Sigma_t^2 + \Sigma_b^2)}} e^{-\Delta\rho^2}. \tag{A3}$$

Here, $c_t = -1$ and $c_b = +1$.

The second-order moments are

$$\langle X_i^2 \rangle = \overline{X}_i^2 + \sigma_{X,i}^2 - c_i \frac{1}{P_{\text{conv}}} \frac{\sigma_{X,i}\rho_0(-\Psi_{X,i}^{\theta}\alpha\sigma_{\theta,i} + \Psi_{X,i}^{S}\beta\sigma_{S,i})}{\sqrt{2\pi(\Sigma_t^2 + \Sigma_b^2)}} \left[2\overline{X}_i - \frac{(\overline{\rho}_t - \overline{\rho}_b)\sigma_{X,i}\rho_0(-\Psi_{X,i}^{\theta}\alpha\sigma_{\theta,i} + \Psi_{X,i}^{S}\beta\sigma_{S,i})}{\Sigma_t^2 + \Sigma_b^2}\right] e^{-\Delta\rho^2},$$

$$\widetilde{X_i^2} = \overline{X}_i^2 + \sigma_{X,i}^2 + c_i \frac{1}{1 - P_{\text{conv}}} \frac{\sigma_{X,i}\rho_0(-\Psi_{X,i}^{\theta}\alpha\sigma_{\theta,i} + \Psi_{X,i}^{S}\beta\sigma_{S,i})}{\sqrt{2\pi(\Sigma_t^2 + \Sigma_b^2)}} \left[2\overline{X}_i - \frac{(\overline{\rho}_t - \overline{\rho}_b)\sigma_{X,i}\rho_0(-\Psi_{X,i}^{\theta}\alpha\sigma_{\theta,i} + \Psi_{X,i}^{S}\beta\sigma_{S,i})}{\Sigma_t^2 + \Sigma_b^2}\right] e^{-\Delta\rho^2},$$

$$\langle X_i Y_j \rangle = \langle X_i \rangle \overline{Y}_j + \overline{X}_i \langle Y_j \rangle - \overline{X}_i \overline{Y}_j + \eta_i \sigma_{X,i}\sigma_{X,j}\delta_{ij} - c_i c_j \frac{1}{P_{\text{conv}}} \frac{(\overline{\rho}_t - \overline{\rho}_b)\sigma_{X,i}\sigma_{Y,j}}{(\Sigma_t^2 + \Sigma_b^2)\sqrt{2\pi(\Sigma_t^2 + \Sigma_b^2)}}$$

$$\times \rho_0^2(-\Psi_{X,i}^{\theta}\alpha\sigma_{\theta,t} + \Psi_{X,i}^{S}\beta\sigma_{S,t})(-\Psi_{Y,j}^{\theta}\alpha\sigma_{\theta,t} + \Psi_{Y,j}^{S}\beta\sigma_{S,t}) e^{-\Delta\rho^2}, \quad \text{and}$$

$$\overline{\theta_i S_i} = \overline{\theta}_i \overline{S}_i + \overline{\theta}_i \widetilde{S}_i + \eta_i \sigma_{\theta,i}\sigma_{S,i} + \frac{1}{1 - P_{\text{conv}}} \frac{(\overline{\rho}_t - \overline{\rho}_b)\sigma_{\theta,i}\sigma_{S,i}}{(\Sigma_t^2 + \Sigma_b^2)\sqrt{2\pi(\Sigma_t^2 + \Sigma_b^2)}} \rho_0^2(-\eta_i\alpha\sigma_{\theta,i} + \beta\sigma_{S,i})(-\alpha\sigma_{\theta,i} + \eta_i\beta\sigma_{S,i}) e^{-\Delta\rho^2}. \tag{A4}$$

From the knowledge of those integrals, variances and covariances are easily calculated.

The solution of the integrals given above is tedious but fairly simple if the following integrals are known:

$$f_1(a, b) = \int_{-\infty}^{\infty} \exp(-x^2)\,\text{erf}(a + bx)\,dx = \sqrt{\pi}\,\text{erf}\left(\frac{a}{\sqrt{b^2 + 1}}\right),$$

$$f_2(a, b) = \int_{-\infty}^{\infty} x\exp(-x^2)\,\text{erf}(a + bx)\,dx = \frac{b}{\sqrt{b^2 + 1}} \exp[-a^2/(b^2 + 1)], \quad \text{and}$$

$$f_3(a, b) = \int_{-\infty}^{\infty} \exp(-x^2)x^2\,\text{erf}(a + bx)\,dx = \frac{\sqrt{\pi}}{2}\,\text{erf}\left(\frac{a}{\sqrt{b^2 + 1}}\right) - \frac{ab^2}{(b^2 + 1)^{3/2}} \exp[-a^2/(b^2 + 1)]. \tag{A5}$$

To solve these integrals [which are not given in Gradshteyn and Ryzhik (2000)] consider, for example, the derivative of f_1 derivative with respect to a, which converts it into a simple double Gaussian whose solution is

$$\frac{\partial f_1}{\partial a} = \int_{-\infty}^{\infty} \exp(-x^2)\, dx \frac{\partial}{\partial a} \operatorname{erf}(a + bx)$$
$$= \frac{2}{\sqrt{b^2 + 1}} \exp[-a^2/(b^2 + 1)]. \tag{A6}$$

Integrating now over a and using the boundary condition $f_1(0, b) = 0$, as when $a = 0$, the integral in Eq. (A5) is an integral of an odd function over a symmetric interval, and we find the above solution.

REFERENCES

Bony, S., and K. Emanuel, 2001: A parameterization of the cloudiness associated with cumulus convection; evaluation using TOGA COARE data. *J. Atmos. Sci.,* **58,** 3158–3183.

Bryan, K., 1969: A numerical method for the study of the circulation of the World Ocean. *J. Comput. Phys.,* **4,** 341–376.

Canuto, V., A. Howard, Y. Chen, and M. Dubovikov, 2001: Ocean turbulence. Part I: One-point closure model—Momentum and heat vertical diffusivities. *J. Phys. Oceanogr.,* **31,** 1413–1426.

——, ——, ——, and ——, 2002: Ocean turbulence. Part II: Vertical diffusivities of momentum, heat, salt, mass, and passive scalars. *J. Phys. Oceanogr.,* **32,** 240–264.

——, ——, P. Hogan, Y. Chen, M. Dubovikov, and L. Montenegro, 2004: Modeling ocean deep convection. *Ocean Modell.,* **7,** 75–95.

Cessi, P., 1996: Grid-scale instability of convective-adjustment schemes. *J. Mar. Res.,* **54,** 407–420.

——, and W. Young, 1996: Some unexpected consequences of the interaction between convective adjustment and horizontal diffusion. *Physica D,* **98,** 287–300.

Chen, L., and W. Young, 1995: Density compensated thermohaline gradients and diapycnal fluxes in the mixed layer. *J. Phys. Oceanogr.,* **25,** 3064–3075.

Conkright, M. E., R. A. Locarnini, H. E. Garcia, T. D. O'Brien, T. P. Boyer, C. Stephens, and J. I. Antonov, 2002: *World Ocean Atlas 2001: Objective Analyses, Data Statistics, and Figures.* CD-ROM documentation, National Oceanographic Data Center, Silver Spring, MD, 17 pp.

DiBattista, M., and A. Majda, 2000: An equilibrium statistical theory for large-scale features of open-ocean convection. *J. Phys. Oceanogr.,* **30,** 1325–1353.

——, ——, and J. Marshall, 2002: A statistical theory for the patchiness of open-ocean deep convection: The effect of preconditioning. *J. Phys. Oceanogr.,* **32,** 599–626.

Ferrari, R., and W. Young, 1997: On the development of thermohaline correlations as a result of nonlinear diffusive parameterizations. *J. Mar. Res.,* **55,** 1069–1101.

Fofonoff, N., 1962: Physical properties of seawater. *The Sea,* M. Hill, Ed., Physical Oceaongraphy, Vol. 1, John Wiley and Sons, 3–30.

Gradshteyn, I., and I. Ryzhik, 2000: *Tables of Integrals, Series and Products.* 6th ed. Academic Press, 1163 pp.

Hirschi, J., J. Sander, and T. Stocker, 1999: Intermittent convection, mixed boundary conditions and the stability of the thermohaline circulation. *Climate Dyn.,* **15,** 277–291.

Jakob, C., and M. Miller, 2004: Parameterization of physical processes: Clouds. *Encyclopedia of Atmospheric Sciences,* J. R. Holton, J. A. Pyle, and J. Curry, Eds., Academic Press, 1692–1698.

Jones, H., and J. Marshall, 1993: Convection with rotation in a neutral ocean: A study of open ocean deep convection. *J. Phys. Oceanogr.,* **23,** 1009–1039.

Kim, S., and A. Stossel, 2001: Impact of subgrid-scale convection on global thermohaline properties and circulation. *J. Phys. Oceanogr.,* **31,** 656–674.

Klinger, B., J. Marshall, and U. Send, 1996: Representation of convective plumes by vertical adjustment. *J. Geophys. Res.,* **101,** 18 175–18 182.

Large, W., J. McWilliams, and S. Doney, 1994: Oceanic vertical mixing: A review and a model with a nonlocal boundary layer parameterization. *Rev. Geophys.,* **32,** 363–403.

Legg, S., and J. Marshall, 1993: A heton model of the spreading phase of open-ocean deep convection. *J. Phys. Oceanogr.,* **23,** 1040–1056.

——, and J. McWilliams, 2000: Temperature and salinity variability in heterogeneous oceanic convection. *J. Phys. Oceanogr.,* **30,** 1188–1206.

Lenderink, G., and R. Haarsma, 1994: Variability and multiple equilibria of the thermohaline circulation associated with deep-water formation. *J. Phys. Oceanogr.,* **24,** 1480–1493.

Lilly, J., P. Rhines, M. Visbeck, R. Davis, J. Lazier, F. Schott, and D. Farmer, 1999: Observing deep convection in the Labrador Sea during winter 1994/1995. *J. Phys. Oceanogr.,* **29,** 2065–2098.

——, ——, F. Schott, K. Lavender, J. Lazier, U. Send, and E. D'Asaro, 2003: Observations of the Labrador Sea eddy field. *Progress in Oceanography,* Vol. 59, Pergamon, 75–176.

Marotzke, J., 1991: Influence of convective adjustment on the stability of the thermohaline circulation. *J. Phys. Oceanogr.,* **21,** 903–907.

Marshall, J., and F. Schott, 1999: Open-ocean convection: Observations, theory, and models. *Rev. Geophys.,* **37,** 1–64.

McDougall, T., 2003: Potential enthalpy: A conservative oceanic variable for evaluating heat content and heat fluxes. *J. Phys. Oceanogr.,* **33,** 945–963.

Mellor, G., and T. Yamada, 1982: Development of a turbulence closure model for geophysical fluid problems. *Rev. Geophys.,* **20,** 851–875.

Rahmstorf, S., 1993: A fast, and complete convection scheme for ocean models. *Ocean Modelling* (unpublished manuscripts), Vol. 101, 9–11.

——, 1995: Multiple convection patterns and thermohaline flow in an idealized OGCM. *J. Climate,* **8,** 3028–3039.

Randall, D., 1989: Cloud parameterization for climate modeling: Status and prospects. *Atmos. Res.,* **23,** 345–361.

Rudnick, D., and R. Ferrari, 1999: Compensation of horizontal temperature and salinity gradients in the ocean mixed layer. *Science,* **283,** 526–529.

Schott, F., M. Visbeck, and U. Send, 1994: Open ocean deep convection, Mediterranean and Greenland Seas. *Ocean Processes in Climate Dynamics,* P. Malafiotte-Rizzoli and A. Robinson, Eds., Kluwer Academic, 203–225.

Send, U., and J. Marshall, 1995: Integral effects of deep convection. *J. Phys. Oceanogr.,* **25,** 855–872.

Titz, S., T. Kuhlbrodt, and U. Feudel, 2004: Grid geometry effects on convection in ocean climate models: A conceptual study. *Ocean Modell.,* **7,** 165–181.

Tompkins, A., 2002: A prognostic parameterization for the subgrid-scale variability of water vapor and clouds in large-scale models and its use to diagnose cloud cover. *J. Atmos. Sci.,* **59,** 1917–1942.

Tziperman, E., and W. Thacker, 1989: An optimal-control adjoint-equations approach to studying the oceanic general circulation. *J. Phys. Oceanogr.,* **19,** 1471–1485.